12. K. Mopper and W. L. Stahovec, *Mar. Chem.* **19**, 305 (1986).
13. G. V. Buxton, C. L. Greenstock, W. P. Helman, A. B. Ross, *J. Phys. Chem. Ref. Data* **17**, 512 (1988).
14. Production rates are used instead of fluxes in order to emphasize differences in ·OH photoproduction potential between different water types. Because of significantly greater light penetration in the open-ocean as compared to coastal waters (*22*), ·OH fluxes are probably similar in these two regions.
15. O. C. Zafiriou, in *Chemical Oceanography*, J. P. Riley and R. Chester, Eds. (Academic Press, London, ed. 2, 1983), vol. 8, pp. 339–379.
16. R. G. Zika *et al.*, *Geochim. Cosmochim. Acta* **49**, 1173 (1985).
17. J. W. Moffett and R. G. Zika, *Environ. Sci. Technol.* **21**, 443 (1987).
18. E. Micinski, J. W. Moffett, O. C. Zafiriou, *Eos* **71**, 171 (1990). We determined that photolysis rates of H_2O_2 in seawater and organic-free distilled water were identical within the analytical error of about 5% (± 1σ SD). Thus, DOM in seawater, and probably other natural waters, does not photosensitize photoproduction of ·OH from H_2O_2.
19. D. Kotzias *et al.*, *Chemosphere* **16**, 1463 (1987); J. Hoigné *et al.*, in *Aquatic Humic Substances: Influence on Fate and Treatment of Pollutants*, I. H. Suffet and P. MacCarthy, Eds. (American Chemical Society, Washington, DC, 1989), pp. 363–381.
20. K. Mopper and R. J. Kieber, unpublished results.
21. Wavelength dependency studies were performed with a Kratos-Schoeffel irradiation system with a 1000-W, continuous-output xenon lamp and a bandwidth of 5 nm. Irradiations were performed for 2 to 8 hours at room temperature with a 10-cm quartz cell. Additional details of experimental conditions are given in (*23*). The data are plotted as action spectrum, that is, ·OH photoproduction per incident photon versus irradiation wavelength [S. E. Broslavsky and K. E. Houk, in *Handbook of Organic Photochemistry*, J. C. Scaino, Ed. (CRC Press, Boca Raton, FL, 1989), vol. 2, pp. 425–468]. The action spectrum was normalized to solar downward irradiance incident at the sea surface (sun zenith angle = 20°, ozone = 0.28 atm-cm, summer, 26°N) in accordance with published procedures: K. S. Baker, R. C. Smith, A. E. S. Green, in *The Role of Solar Ultraviolet Radiation in Marine Ecosystem*, J. Calkins, Ed. (Plenum, New York, 1982), pp. 79–91; R. G. Zepp, G. Z. Baughman, P. F. Scholtzhauer, *Chemosphere* **10**, 119 (1981).
22. R. C. Smith and K. S. Baker, *Photochem. Photobiol.* **29**, 311 (1979).
23. R. J. Kieber, X. Zhou, K. Mopper, *Limnol. Oceanogr.*, in press. The production rate of LMW carbonyl compounds formed during irradiation (photolysis) of DOM was found to decrease in direct proportion to the rate of photobleaching (loss) of absorbance by DOM in natural water samples. Preliminary results indicated that a similar relation exists between ·OH photoproduction and absorbance photobleaching (*24*).
24. X. Zhou and K. Mopper, unpublished results.
25. At the pH of seawater (~8.2), reaction of chloride with ·OH can be neglected because of its nearly complete reversibility; however, in acidic media (that is, pH <3), this reaction proceeds at a significant rate [O. C. Zafiriou, M. B. True, E. Hayon, in *Photochemistry of Environmental Aquatic Systems*, R. G. Zika and W. J. Cooper, Eds. (American Chemical Society, Washington, DC, 1987), pp. 89–105, and references cited therein].
26. Y. Sugimura and Y. Suzuki, *Mar. Chem.* **241**, 105 (1988); J. R. Toggweiler, *Nature* **334**, 468 (1988).
27. K. Mopper, R. G. Zika, A. M. Fischer, in *Humic Substances: IV*, P. MacCarthy, E. T. Gjessing, R. F. C. Mantoura, P. Sequi, Eds. (Wiley-Interscience, New York, in press).
28. D. J. Kieber, J. McDaniel, K. Mopper, *Nature* **341**, 637 (1989); A. Geller, *Limnol. Oceanogr.* **31**, 755 (1986).
29. J. H. Ryther, *Science* **166**, 72 (1969).
30. P. M. Williams and E. R. M. Druffel, *Nature* **330**, 246 (1987).
31. J. A. Fuhrman, T. D. Sleeter, C. A. Carlson, L. M. Proctor, *Mar. Ecol. Prog. Ser.* **67**, 207 (1989).
32. B. Halliwell, J. M. C. Gutteridge, O. I. Aruoma, *Anal. Biochem.* **165**, 215 (1987).
33. T. Mill, W. Haag, D. Karentz, in "Effects of solar ultraviolet radiation on biogeochemical dynamics in aquatic environments," N. V. Blough and R. G. Zepp, Eds. (Woods Hole Oceanographic Institution Technical Report 90-09, Woods Hole, MA, 1990), pp. 89–93.
34. B. Halliwell and J. M. C. Gutteridge, *Free Radicals in Biology and Medicine* (Oxford Univ. Press, New York, ed. 2, 1989).
35. R. C. Smith and K. S. Baker, *Science* **208**, 592 (1980).

36. We thank T. Mill, O. C. Zafiriou, J. M. C. Plane, E. S. Saltzman, N. V. Blough, M. Ehrhardt, C. Langford, R. G. Zika, and D. J. Kieber, for discussions of the data and R. J. Kieber for measurement of the action spectrum. Financial support was provided by the National Science Foundation's Chemical Oceanography Program (OCE86-13940 and OCE89-17709) and the Office of Naval Research's Ocean Chemistry Program (N0014-87-G0116).

27 April 1990; accepted 23 July 1990

Intercalation of Sea Urchin Proteins in Calcite: Study of a Crystalline Composite Material

AMIR BERMAN, LIA ADDADI, ÅKE KVICK, LESLIE LEISEROWITZ, MITCH NELSON, STEPHEN WEINER

Sea urchin skeletal elements are composed of single crystals of calcite. Unlike their synthetic counterparts, these crystals do not have well-developed cleavage and are consequently much more resistant to fracture. This phenomenon is due in part to the presence of acidic glycoproteins occluded within the crystals. By means of x-ray diffraction with synchrotron radiation, it is shown that the presence of the protein in synthetic calcite only slightly decreases the coherence length but significantly increases the angular spread of perfect domains of the crystals. In biogenic calcite, the coherence length is 1/3 to 1/4 as much as that in synthetic calcite and the angular spread is 20 to 50 times as wide. It is proposed that the presence of macromolecules concentrated at mosaic boundaries that are oblique to cleavage planes is responsible for the change in fracture properties. These results may be important in the material sciences, because of the unusual nature of this material, namely, a composite based on the controlled intercalation of macromolecules inside single-crystal lattices.

THE MINERAL PHASE OF SEA URCHIN spines and tests is composed of fenestrated Mg-bearing calcite. It is a unique material, as whole body plates and spines up to several centimeters in length diffract x-rays as single crystals. These skeletal elements are not, however, as fragile as single calcite crystals but appear to be made of a relatively strong material (*1*). Pure calcite cleaves easily along the well-developed {104} crystal planes. Sea urchin skeletal elements, however, break with conchoidal (glassy) fracture, typical of amorphous materials. The protein content of these skeletal elements is of the order of 0.5 mg per gram of calcite (*2, 3*). The possibility that organic macromolecules located within the crystals are responsible for the unusual fracture properties was first proposed by Merker (*4*). Direct experimental evidence supporting this proposal was obtained when calcite crystals were grown in the presence of acidic glycoproteins extracted from sea urchin skeletons (*5*). The macromolecules intercalate into single synthetic crystals, and, as a result, their fracture properties change. These protein-crystal composites break with conchoidal fractures similar to those of fractured sea urchin skeletal elements (*5*). The molecular structure of echinoderm skeletal elements may therefore be of interest to material scientists, as these materials are composed of large single crystals reinforced by proteins located within their lattice structure.

The aim of this study was to gain insight into this unique protein-crystal composite by determining how bulky proteins can be incorporated into single crystals. As calcite crystals are extremely well ordered, it was necessary to examine their x-ray diffraction profiles with the use of highly collimated synchrotron radiation. The study focuses on the internal texture of biogenic and synthetic calcite crystals, in terms of the mosaic spread and the domain size of the crystals. The following crystals were analyzed: two pure calcite crystals; three calcite crystals containing occluded protein ranging in concentration from approximately 250 to 750 ppm (w/w) (*6*); two small sea urchin spines and one sea urchin tooth element (*7*). The diffraction data were collected at the National Synchrotron Light Source (Brookhaven

A. Berman and S. Weiner, Department of Isotope Research, Weizmann Institute of Science, Rehovot, 76100, Israel.
L. Addadi and L. Leiserowitz, Department of Structural Chemistry, Weizmann Institute of Science, Rehovot, 76100, Israel.
Å. Kvick and M. Nelson, Chemistry Department, Brookhaven National Laboratory, Upton, NY 11973.

National Laboratory) on beam line X7B (*8*). Two sets of diffraction profiles were collected for a series of *hkl* reflections in the ω and ω/2θ modes (see definitions in Fig. 1). An analyzer crystal, introduced in front of the detector, makes possible separate measurements of the coherence length (the size of perfectly ordered crystalline domains) from ω/2θ reflection profiles, and of the mosaic spread (the misalignment of perfect domains) from the ω reflection profiles. Representative reflections of ω and ω/2θ scans are shown in Fig. 1, A and B, respectively.

The profiles of the ω scans for the spine and the crystals containing sea urchin protein are much broader than those of the ω/2θ scans indicating true mosaic misalignment (*9*). Figure 1, C through E, depicts the full width at half maximum (FWHM) of the two scan types as a function of θ for a series of *hkl* reflections derived from three crystals. The ω scan widths vary from 0.004° ± 0.001° for the pure crystal (Fig. 1C), to 0.03° ± 0.01° for the sea urchin–affected crystal (Fig. 1D), to 0.15° ± 0.03° for the spine (Fig. 1E). The ω/2θ scan widths range from 0.003° at low θ to 0.013° at high θ for the pure crystal (Fig. 1C); from 0.005° to 0.018° for the sea urchin–affected crystal (Fig. 1D), and from 0.015° to 0.043° for the spine (Fig. 1E). If we apply the Scherrer formula (*10*), we find that these values correspond to average domain sizes of 500 ± 100, 450 ± 150, and 150 ± 50 nm, respectively (Fig. 2). The tooth element, for which only two reflections were measured, gave ω/2θ values comparable to those of the spine, but the ω scans were threefold sharper. Part of the peak broadening in the spine and the tooth element, but not in the synthetic crystals, may be due to the presence of Mg. We cannot at this stage evaluate exactly the contribution of this factor, although we do note that the ω/2θ profiles for the spine and the tooth element have, in addition, pronounced wings (Fig. 1B) (*11*).

The observed changes in morphology of the sea urchin–affected crystals upon growth in the presence of the protein indicated preferential adsorption on the {1$\bar{1}$0} faces (*5*). We therefore looked for anisotropic effects on the mosaic spread by performing ω scans on certain reflections at different ψ angles (the angle of rotation of the crystal around its diffraction vector). We did not observe any systematic differences for a specimen with a protein content of about 250 ppm, probably because of the high symmetry (hexagonal) of calcite, resulting in sixfold degeneracy for each *hkl* plane. The diffraction profiles from the crystals with a protein content of as much as 750 ppm are, however, often composed of well-defined, very sharp subpeaks. The profiles of the subpeaks change for different values of ψ (Fig. 3). Insufficient data are available to determine whether a correlation exists between the observed anisotropy and the crystal architecture and orientation.

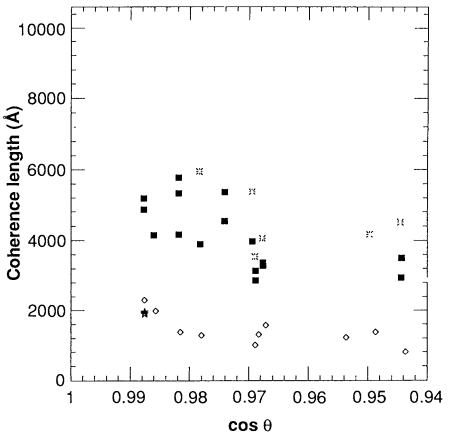

Fig. 2. Coherence length calculated from sets of ω/2θ profiles according to the Scherrer formula (*10*) for four specimen crystals: (*) pure calcite; (■) sea urchin–affected synthetic calcite; (◇) spine; (★) sea urchin tooth element. For the pure crystal, the values of FWHM of the peaks at lower θ were discarded because their width (~0.003°) is at the resolution limit.

The results clearly demonstrate that the presence of these proteins within the crystal does alter the crystal texture as follows. (i) There is a relatively small reduction in the domain size of the sea urchin–affected crystal relative to that of the pure calcite. (ii) There is a dramatic increase of the angular spread of the blocks in these crystals. (iii) When the amount of occluded protein exceeds a certain value, the continuous distribution of domains within the crystal no

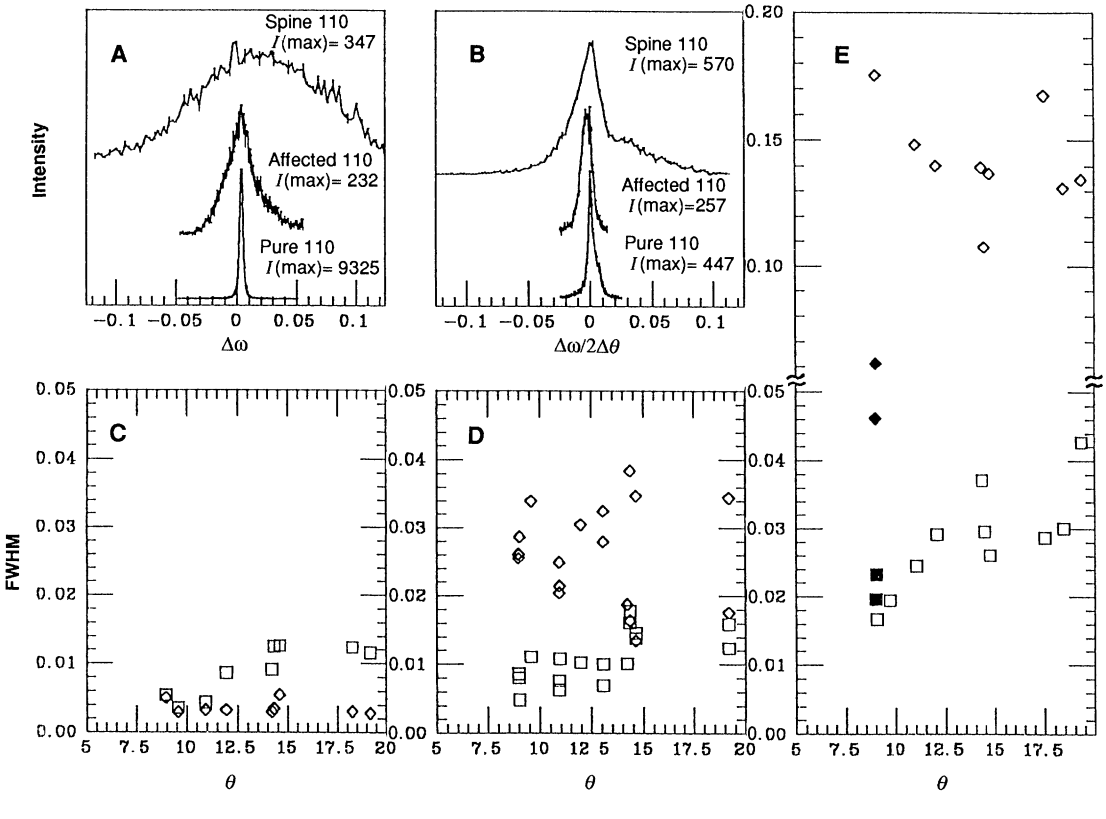

Fig. 1. Representative profiles of diffraction peaks from the same crystallographic plane, 110, of the three different types of examined crystals: (**A**) ω scans. (**B**) ω/2θ scans. The unit of intensity is counts. Plots of FWHM versus Bragg angle θ of a set of measured reflections (λ = 0.945 Å): (**C**) synthetic pure calcite; (**D**) synthetic calcite with occluded sea urchin protein; (**E**) sea urchin spine. (□) ω/2θ scans; (◇) ω scans; (■) and (◆) refer to the tooth element (note change of scale above 0.05). The *hkl* indices of the measured reflections in order of increasing θ are 104, 006, 110, 113, 022, 024, 018, 1 0 10, 119, and 300. In an ω scan, only the crystal is rotated by an angle Δω about the main axis of the diffractometer, which is perpendicular to the diffraction plane; the detector is kept fixed at the Bragg angle 2θ. In an ω/2θ scan, the crystal is rotated by Δω and the detector by 2Δθ, where Δω = Δθ. Note that the ω and 2θ axes coincide. Error bars = $\sqrt{I}$.

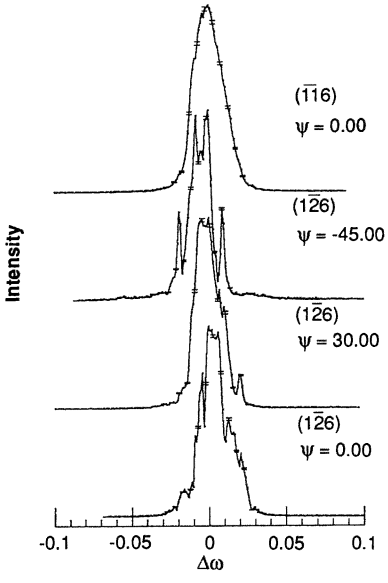

Fig. 3. Typical profiles of diffraction peaks of calcite crystals grown in the presence of a high protein concentration (8.0 μg/ml) (λ = 1.3556 Å). The profiles are from the plane (1̄16) and from the plane (12̄6) at different ψ angles (calcite space group is $\bar{R}3c$. In order to determine the relative configurations of the crystal axes and the nondiffracting planes to the incident beam at every ψ angle, the diffractometer angles were transformed to the crystal system through orientation and rotation matrices multiplication, as derived from International Tables for X-ray Crystallography (*16*) (results not shown). Some peaks are smooth and others are dentated, an indication of anisotropy in the interference of the adsorbed macromolecules with homogeneous crystal growth. The step-to-step resolution of these profiles is 0.001°. Error bars = $\sqrt{I}$.

longer exists, and the crystal is divided into a few distinct blocks, which still, however, display a very good coherence. This phenomenon is not observed from all directions, indicating an anisotropic effect due to protein adsorption. (iv) The sea urchin spine domains are smaller and have wider angular distribution than synthetic calcite crystals with occluded protein. (v) A single sea urchin tooth element has domains similar in size to those of the spine.

It is evident that bulky proteins cannot be accommodated inside perfect lattice domains but must create a discontinuity at the site of adsorption. A simple calculation (*12*) shows that the average distance between macromolecules must be about 15 nm if a homogeneous distribution of proteins is assumed. Our crystallographic measurements, however, show that the synthetic crystals with occluded protein have domain sizes of about 400 nm. We, therefore, conclude that the macromolecules must be concentrated at the mosaic block boundaries. An extension of the calculation (*13*) suggests that roughly 20 ± 10% of the block's surfaces are covered by proteins. It is the presence of these macromolecules on the block boundaries that accounts for the observed changes.

An unexpected observation is that, at high protein concentrations within the crystal, certain reflections break up into subpeaks. These subpeaks, measured by ω scans, represent slightly misaligned "superblocks" or crystallites. An evaluation of the integrated intensities of the subpeaks, relative to the total integrated intensity, indicates that each of these crystallites may constitute up to 2% of the total crystal volume. We do not know the exact manner by which the proteins cause all these changes, but it must be somehow involved in the inhibition of certain active growth sites on the crystal surface. Temporary inhibition of growth at a certain site could then conceivably induce further adsorption of protein at the same site, requiring that growth be resumed at a different location. The presence of the protein at block boundaries certainly exaggerates the nature of the boundary itself. Although we did not succeed by using x-rays in determining that the proteins are anisotropically distributed on those boundaries, we know from an earlier study (*5*) that the proteins are preferentially adsorbed from solution on the {1̄10} planes of calcite crystals during growth. On the basis of these observations and the diffraction data, we propose that the proteins, located at the boundaries of quasi-perfect mosaic blocks, generate and stabilize discontinuities at the submicrometer level. The presence of these macromolecules mainly on boundaries oblique to cleavage planes interferes with the propagation of a smooth fracture. In addition, the increased angular spread may also contribute to impairing the cleavage. If proven general, this principle may well have broader application to the material sciences as a means of creating new single crystalline composites intercalated by specifically adsorbed intracrystalline polymers.

Two reflections of a single fibrous element from a sea urchin tooth were also measured. This element is much smaller than the spine and may represent the product of a single nucleation event inside one syncytial vesicle. The domain sizes of the tooth element are similar to those of the spine, but the angular dispersion is only about one-third of that measured in the spine (Fig. 2). This suggests that domain size is an intrinsic feature of the echinoid skeletal mineral phase. The greater angular dispersion of the spines, however, could reflect an accumulation of misalignments due to the biological "assembly" process involving the fusion of multiple skeletal elements formed in different vesicles. Moreover, electron microscope studies of fracture surfaces of echinoderm skeletal elements have revealed microstriae, needles, and laths about 200 nm wide (*14*), or small whisker-shaped crystallites (*15*) with average dimensions of 360 by 130 nm. These values are similar to the average coherence lengths of the sea urchin spine, namely, 150 ± 50 nm. We do, however, emphasize that the misalignments measured here are still exceedingly small, and the mystery of how the sea urchin constructs a macroscopic, almost "perfect," single crystal, still remains.

REFERENCES AND NOTES

1. J. Weber, R. Greer, B. Voight, E. White, R. Roy, *J Ultrastr. Res.* **26**, 355 (1969); J. D. Currey, *J. Mar. Biol. Assoc. U.K.* **55**, 419 (1975); R. B. Emlet, *Biol Bull. (Woods Hole)* **163**, 264 (1982); A. Burkhardt, W. Hansmann, K. Markel, H. J. Niemann, *Zoomorphology (Berl.)* **102**, 189 (1983).
2. S. Weiner, *J. Exp. Zool.* **234**, 7 (1985).
3. D. M. Swift, C. S. Sikes, A. P. Wheeler, *ibid* **240**, 65 (1986).
4. E. Merker, *Zool. Jahrb. Abt. Allg. Physiol. Tiere* **36**, 25 (1916).
5. A. Berman, L. Addadi, S. Weiner, *Nature* **331**, 546 (1988).
6. Sea urchin acidic glycoproteins that are intimately associated with the mineral phase of *Paracentrotus lividus* (eastern Mediterranean) were extracted as described by Weiner (*2*). Calcite crystals were grown in the presence of the glycoproteins (composition: Asp, 13%; Glu, 15%; Gly, 17%; Ala, 10%; and Pro, 8%) as described by Berman *et al.* (*5*). The concentration of occluded material in the crystals ranges from below the detection limit to more than 1000 ppm (*5*), depending on the protein concentration in the crystallization solution. The synthetic crystals were approximately equidimensional (150 μm). The sea urchin spine dimensions are ~80 by 800 μm, and the Mg content, estimated from the reduction in cell dimensions, is 5% (*17*).
7. Sea urchin teeth are calcitic polycrystalline complex assemblies of several elements (*18*): "primary" and "side" plates, and calcareous fibers, each of which is a single crystal. A fibrous element from the central zone of the tooth from a region that is not cemented was used. The dimensions of the tooth element are approximately 15 by 150 μm; the estimated Mg content from literature data (*18, 19*) is 15% and from direct measurements of the cell dimensions is 8 to 10%.
8. The beam line is instrumented with a Huber six-circle diffractometer and a scintillation detector, with detector motion in the vertical plane (Å. Kvick, unpublished data). The x-ray beam is obtained by monochromatization of the bending magnet radiation with a Si(111) double-crystal monochromator followed by focusing in the horizontal direction with a Rh-coated mirror at a grazing angle of 3 mrad (*20*). The energy resolution at a wavelength λ = 0.945 Å with the optics used was $\Delta\lambda/\lambda \approx 8 \times 10^{-4}$. A Ge(220) analyzer crystal was installed in front of the detector; this analyzer crystal operates as a very narrow slit that provides the necessary resolution in the ω/2θ scans and deconvolutes the contribution of θ from ω scans. The angular resolution, defined by the x-ray beam crossfire, is 0.003° or less.
9. Had the ω profiles been sharper than the corresponding ω/2θ profiles, it would not be possible to exactly evaluate the mosaic spread.
10. A Guinier, *X-ray Diffraction in Crystals, Imperfect Crystals, and Amorphous Bodies* (Freeman, San Francisco, 1963), p. 124.
11. X. B. Kan, M. E. Misenheimer, K. Forster, S. C. Moss, *Acta Crystallogr. Sect. A* **34**, 418 (1987).
12. The assumptions behind the calculation are as follows: (i) it is estimated that an average of 100 amino acid residues are present per protein molecule; and (ii) a protein concentration (by weight) of 500 ppm is based on protein measurements performed by high-performance liquid chromatography (*5*). This

yields 30 protein molecules per million calcite unit cells.
13. The volume of a coherence block is 4000^3 Å^3. The volume of a single calcite unit cell is $\sin 60 \times 5 \times 5 \times 17$ Å^3. Hence, a total of 200×10^6 unit cells in one block are surrounded by ~6000 protein molecules (*12*). If we assume two-dimensional β-pleated sheet dimensions, the coverage (protein/mineral ratio) is of the order of 20% for an average value of the intracrystalline protein concentration.
14. K. M. Towe, *Science* **157**, 1048 (1967).
15. P. L. O'Neill, *ibid.* **213**, 646 (1981).
16. *International Tables for X-ray Crystallography* (Kynoch, Birmingham, United Kingdom, 1974), vol. 4, p. 277.
17. F. Lippmann, *Sedimentary Carbonate Minerals* (Springer-Verlag, New York, 1973), pp. 43–47.
18. K. Markel, P. Gorny, K. Abraham, *Fortschr. Zool.* **24**, 103 (1977).
19. J. H. Schroeder, E. J. Dwornik, J. J. Papike, *Geol. Soc. Am. Bull.* **80**, 1613 (1969).
20. J. B. Hastings, P. Sourtti, W. Thomlinson, Å. Kvick, T. F. Koetzle, *Nucl. Instrum. Methods* **208**, 55 (1983).
21. We thank F. Frolow for assistance with the crystallographic measurements performed at the Weizmann Institute of Science. This work was performed in part at the Brookhaven National Laboratory under contract DE-AC02-76-CH00016 with the U.S. Department of Energy and supported by its Division of Chemical Sciences, Office of Basic Energy Sciences.

26 April 1990; accepted 8 August 1990

The Origin of Crustacean Biramous Appendages and the Evolution of Arthropoda

MICHAEL J. EMERSON AND FREDERICK R. SCHRAM

The evolution of biramous appendages in crustaceans is central to the debate on the origin of the arthropods. It is proposed that the biramous limb evolved through the basal fusion of adjacent pairs of ancestrally uniramous appendages. As a result, the existing system of homology, in which uniramous and biramous appendages are considered equivalent, may be invalid. Similarly, the homology of individual body segments between uniramians, such as insects and myriapods, and arthropod groups with biramous limbs is also called into question. Two uniramian segments, or a diplosegment, may be homologous to a single body segment in biramous groups.

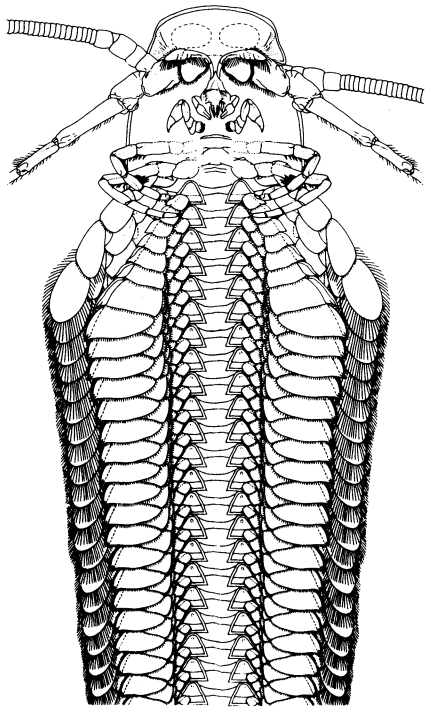

Fig. 1. Ventral reconstruction of *Tesnusocaris goldichi* based on all currently available specimens. The head, with its raptorial postmandibular mouthparts, is v[illegible] remipedes.

CENTRAL TO THE DEBATE ON ARthropod phylogeny is the relation of the insects and myriapods with uniramous limbs to the arthropods with biramous limbs such as crustaceans, cheliceriforms, and a wide range of Paleozoic fossils including trilobites. Among the extant groups of biramous arthropods, the crustaceans appear to be less derived than the cheliceriforms (*1*) and may be close to a common ancestor with the uniramians. The relation between Uniramia and Crustacea is critical because these groups share such characters as mandibles and a similar cephalic composition that are interpreted either as evidence of a monophylectic origin (*2*), or as convergent evolution of features in unrelated groups (*3*). However, any attempt to create a phylogeny of the arthropods must deal with the question of the origin of biramous limbs.

Some investigators have suggested that biramous limbs arose from uniramous ones through the gradual evolution of an appendicular structure, such as the stylus of some insect legs, into the exopod of the typical biramous appendage (*4*). However, lack of intermediate forms and the extreme variability of such auxiliary limb structures would seem to argue against this hypothesis. Another approach has been to start with biramous (or polyramous) limbs and delete the outer exopod and the basal accessory epipodites to derive a secondarily uniramous limb (*5*). However, this suggestion not only begs the question of the ancestry of the biramous limb, but also minimizes evidence that the resemblance between primary and secondary uniramous limbs is convergent. The failure of such theories to account satisfactorily for the evolution of biramous limbs has been one of the factors leading some authors to conclude that the arthropods are diphylectic or polyphylectic (*3*). Many investigators, however, argue that the proposition that each arthropod group evolved their numerous shared, derived characters independently strains credulity (*2*).

Newly discovered fossils of a problematic Mississippian arthropod, *Tesnusocaris goldichi* (*6*), provide anatomical insights that prove crucial to understanding this species (*7, 8*) as well as suggest a new hypothesis for the events of arthropod history. The structure of the head (Fig. 1) confirms a sister group relation of this fossil species to living nectiopodan remipede crustaceans (*9*). The trunk of *Tesnusocaris* also resembles those of extant remipedes in that regionalization of the segments and trunk limbs is absent, but an examination of the locomotory appendages of the fossils reveals a structure quite different from that of Nectiopoda and other crustaceans (Fig. 2C). Instead of the typical, biramous appendages that were expected, we found two distinct sets of uniramous limbs on each segment. There is a midventral series, which may be unique among arthropod limbs in that they appear to be adapted for sculling (*8*). In addition, there is a ventrolateral series of fairly typical swimming limbs, adapted for rowing.

Detailed study of the fossils, as outlined below, suggests that these are two separate sets of uniramous limbs and not the remnants of a biramous limb whose protopodal base has fused into the body wall. (i) The wide separation of the medially situated limbs and laterally positioned appendages on our fossils seems too great to suggest that they were ever associated with a common protopod. (ii) The great differences between the apparent function of the two sets of limbs (*8*) suggest that they evolved separately and that they possessed distinct musculatures. (iii) The first segments of both sets of limbs resemble true coxae seen in various arthropods, rather than the mobile podites typical of the more distal parts of limbs that might be expected if the original coxa had been fused to the body wall. (iv) A comparison of the number of podomeres on the

San Diego Natural History Museum, San Diego, CA 92112.